He, Shichao; Wilson, Benjamin P.; Lundström, Mari; Liu, Zhihong

Hazard-free treatment of electrolytic manganese residue and recovery of manganese using low temperature roasting-water washing process

Published in:
Journal of Hazardous Materials

DOI:
10.1016/j.jhazmat.2020.123561

Published: 15/01/2021

Document Version
Peer-reviewed accepted author manuscript, also known as Final accepted manuscript or Post-print

Journal Pre-proof

Hazard-free treatment of electrolytic manganese residue and recovery of manganese using low temperature roasting-water washing process

Shichao He (Conceptualization) (Methodology) (Software) (Investigation) (Data curation) (Writing - original draft), Benjamin P. Wilson (Writing - review and editing), Mari Lundström (Writing - review and editing), Zhihong Liu (Resources) (Writing - review and editing) (Supervision) (Data curation)

PII: S0304-3894(20)31547-8

DOI: https://doi.org/10.1016/j.jhazmat.2020.123561

Reference: HAZMAT 123561

To appear in: *Journal of Hazardous Materials*

Received Date: 26 February 2020

Revised Date: 20 July 2020

Accepted Date: 21 July 2020

Please cite this article as: He S, Wilson BP, Lundström M, Liu Z, Hazard-free treatment of electrolytic manganese residue and recovery of manganese using low temperature roasting-water washing process, *Journal of Hazardous Materials* (2020), doi: https://doi.org/10.1016/j.jhazmat.2020.123561

Hazard-free treatment of electrolytic manganese residue and recovery of manganese using low temperature roasting-water washing process

Shichao He [a], Benjamin P. Wilson [b], Mari Lundström [b], Zhihong Liu [a]*

[a] *School of Metallurgy and Environment, Central South University, Changsha 410083, China*

[b] *Hydrometallurgy and Corrosion, Department of Chemical and Metallurgical Engineering (CMET), School of Chemical Engineering, Aalto University, P.O. Box 16200, FI-00076 AALTO, Finland*

* Corresponding author at: School of Metallurgy and Environment, Central South University, Changsha 410083, PR China.

Tel: +86 731 88830923, E-mail address: zhliu@mail.csu.edu.cn (Zhihong Liu)

Graphic abstract

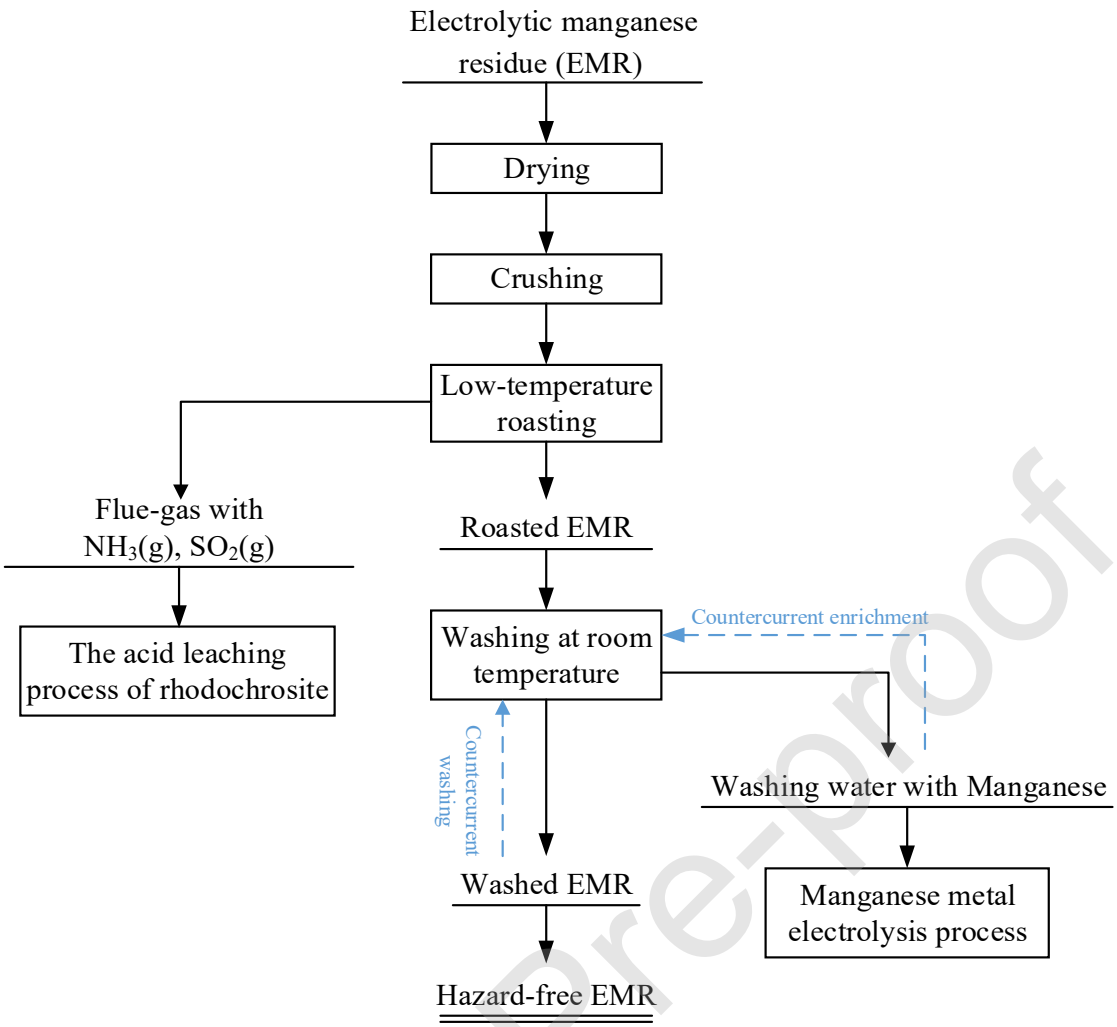

Highlights

- A process for hazard-free treatment electrolytic manganese residue (EMR) was proposed;
- Almost all of the ammonia in the EMR was recovered by low-temperature roasting;
- The manganese present in the EMR could be recovered by countercurrent water-washing;
- The toxicity leaching results of the EMR after hazard-free treatment met GB 8978-1996.

Abstract

A combined low-temperature-roasting and water-washing process is investigated as a hazard-free method to treat electrolytic manganese residue (EMR) and recover manganese. In this study, the phase transformation characteristics and a thermodynamics analysis of the low temperature roasting process of EMR are evaluated. In addition, the effects of temperature and time on the phase transformation of EMR in the roasting process and the washing characteristics of roasted EMR samples are also investigated. Results reveal that some unstable phases within EMR are transformed into more stable phases depending on the treatment time/temperature conditions used and EMR roasted for 60 min at 600 °C ($R_{60min/600°C}$) exhibit the highest rate of manganese recovery, 67.12 %. After 25 minutes of deionized water washing, the concentration of manganese in solution from $R_{60min/600°C}$ material become stable, whereas after 6 washing cycles the concentration of manganese in the solution is < 0.005 g/L. The $R_{60min/600°C}$ material with three wash cycles results in a manganese-water solution concentration that is suitable for use in electrolytic manganese metal production. Finally, toxicity leaching tests show that the concentrations of ions present in the leaching solution are all lower than the regulatory limits mandated by the Chinese Integrated Wastewater Discharge Standard GB 8978-1996.

Keywords: Electrolytic manganese residue (EMR); Hazard-free treatment; Low temperature roasting; Water washing; Recovery of manganese

1. Introduction

Electrolytic manganese is primarily used in the production of alloy steels, non-ferrous alloys and rechargeable batteries. China is currently the largest manufacturer of electrolytic manganese with an annual production of over one million tons, which

accounts for approximately 98% of global output (Tan et al., 2005; Xu et al., 2014; Zhou et al., 2014; Shu et al., 2016a; Li et al., 2016). China's smelters of electrolytic manganese are mainly concentrated in the famous "manganese triangle" - an area bounded by Hunan province, Guizhou province and Chongqing City – with additional plants in the Guangxi Zhuang and Ningxia Hui Autonomous Regions (Duan et al., 2009; Shu et al., 2019a). All these areas have vulnerable and complex ecologies, consequently there is a strong requirement for good environmental practice (Zhang and Cheng, 2007; Hagelstein, 2009; Lu et al., 2014).

In China, electrolytic manganese is produced by a traditional sulfuric acid leaching-electrowinning process, which uses rhodochrosite ore as the primary raw material (Zhang and Cheng, 2007). The overall process typically involves the following steps (Xu et al., 2014; Brantley and Rampacek, 1968; Duan et al., 2011): (1) sulfuric acid solution and rhodochrosite ore are mixed in a slurry in a tank and stirred for 3-6 hours to achieve leaching; (2) Stoichiometric amounts of pyrolusite ore is added to the slurry to oxidize the dissolved ferrous ions, which are then subsequently precipitated as ammonium hydroxide additions as slurry pH is increase to 6.5-7.0; (3) Cu(II), Co(II), Ni(II), Cr(III) and other heavy metals ions present are precipitated as the corresponding sulfide by addition of sodium dimethyl dithiocarbamate (SDD) to the slurry; (4) Following separation, the solution is sent to electrowinning tanks for electrolytic manganese production and the electrolytic manganese residue (EMR) is stockpiled in waste dumps (Wang et al., 2013). Currently, about 10 to 12 tons of EMR is produced for every ton of electrolytic manganese metal and this level of waste is rising rapidly due to the continued decrease in global rhodochrosite ore grade quality (Shu et al., 2016b; Shu et al., 2016c; Shu et al., 2018a).

Black-mud-like EMR has a water content between 25 to 35 wt.% and a pH range of 5.0 to 6.5. In addition, EMR contains not only a significant amount of soluble salts like ammonium sulfate and manganese sulfate, but also heavy metal elements that include Ni, Co, Cd, Pb, Cu amongst others (Xin et al., 2011; Du et al. 2014). At present, Chinese

electrolytic manganese smelters - without exception - dispose of their EMR in designated waste dumps, however, this not only consumes considerable areas of land, but also results in significant pollution of the surrounding soil and groundwater (Duan et al., 2009; Hou et al., 2012; Xu et al., 2014). In addition, as the stockpiled EMR is generally exposed to the open air, inevitably metal sulfide and ammonium sulfate decomposition takes place in the presence of sunlight, oxygen and bacteria that result in harmful gases emissions (e.g. SO_2 and NH_3) to the surrounding atmosphere (Li et al., 2015).

With increasingly stringent environmental regulations in China, the ability to treat EMR in hazard-free way has become of critical importance and over the last decade, a number of related studies have been carried out (Xin et al., 2011; Du et al. 2014; Xu et al., 2014; Yang et al., 2014; Li et al., 2015; Shu et al., 2016b; Shu et al., 2016c; Wu et al., 2016; Li et al., 2018; Shu et al., 2018a; Shu et al., 2019b; Shu et al., 2018b). These investigations can be roughly divided into four main categories:

(1) Recovery of manganese and ammonia nitrogen from EMR - Shu et al. (Shu et al., 2019b) optimized the simultaneous removal of manganese and ammonia nitrogen from EMR through chemical precipitation based on N to P molar ratios and pH. Over 99% of the manganese was removed primarily as either $MnHPO_4 \cdot 3H_2O$ or manganite, whilst more than 96% of the ammonia nitrogen was precipitated as struvite ($Mg(NH_4)PO_4 \cdot 6H_2O$) at pH 9.5 with a N to P molar ratio of 1:1.15. Bioleaching with pyrite-leaching and sulfur-oxidizing bacteria has also been studied for manganese removal with removal efficiencies of 81% and 93% achieved after 9 days (Xin et al., 2011).

(2) Use in building materials - sulfur concrete production where EMR was used as a filler along with modified sulfur and river sand aggregate has been investigated (Yang et al., 2014). Results showed that the concrete obtained had good compressive (49-63 MPa) and bending (7.1-9.5 MPa) strengths as well as good at penetration resistance to acidic or alkali solutions. Related research into the production of steam-autoclaved

bricks using, 10.5-12 wt. % cement, quicklime, river sand and 30-40 wt. % EMR as raw materials showed that EMR additions resulted in higher compressive strengths and lower dry shrinkage, without any related environmental toxicity issues (Du et al. 2014). EMR has also been used in the preparation of porous ceramics in combination with carbon powder, dolomite and kaolin to obtain material high apparent porosity (~70%), compressive strength (7MPa) and acidity-alkali stability (Wu et al., 2016). Production of quasi-sulfoaluminate cement (Q-SAC) by calcination of EMR (up to 40 wt. %), limestone and kaolin at approximate 1200 °C created cements with compressive strengths between 35-65 MPa, which were found to be further improved by the addition of gypsum (Hou et al., 2012).

(3) Wastewater and soil remediation treatments - A modified EMR adsorbent that was effective for the removal of methylene blue from wastewater was prepared via hydrothermal treatment from a mixed slurry of EMR, magnesium chloride and sodium silicate solution by Shu et al. (Shu et al., 2018b). In contrast, an activated EMR soil remediation agent was synthesized by ball milling and calcining a mixture of $NaCO_3$ to EMR at 900 °C for 120 minutes (Li et al., 2018). After preparation, the effective silica content in the activated EMR increased significantly (from 0.19 to 12.6%) and resultant material was found to aid the remediation of soil contaminated by heavy metals.

(4) Stabilization/solidification - Shu et al. (Shu et al., 2018a) studied the solidification of the Mn^{2+} and NH_4^+ present in EMR by addition of MgO and various phosphates at different Mg to P molar ratios. Analysis of the process, determined that the Mn^{2+} was mainly stabilized in the form of $Mn(H_2PO_4)_2 \cdot 2H_2O$, $Mn_3(PO_4)_2 \cdot 3H_2O$, $Mn(OH)_2$, and MnOOH, whereas the NH_4^+ solidified primarily as $NH_4MgPO_4 \cdot 6H_2O$.

Although, a majority of the EMR related studies have led to the development of hazard-free EMR treatment technologies, none of these processes are so far in commercial use due to the need for high levels of additional materials, which results in high costs and additional waste streams. Low-temperature roasting (Mu et al., 2018; Khanlariana et al., 2019), is an eco-friendly and low-cost process that has been widely used for the

treatment of various industrial solid wastes (Li et al., 2014; Cui et al., 2018) and the recovery of valuable materials from secondary resources (Li et al., 2017; Aleksandrov et al., 2017; Aleksandrov et al., 2019; Liu et al., 2019). In this work, a combined low temperature roasting-water washing process was studied for the hazard-free treatment of EMR material. This methodology was selected based on the EMR chemical and phase compositions and had the following goals: (1) A post-process EMR that is harmless and can be stockpiled without causing environmental damage; (2) During the treatment process, almost all of the ammonia and manganese are recovered; (3) Treated EMR has the potential to be used in building materials (Hou et al., 2012; Du et al. 2014; Shu et al., 2016a).

2. Experimental

2.1 Materials

The EMR used in this study was provided by an electrolytic manganese smelter from the Xiushan Region, China. Prior to use, EMR material was dried in an oven at 105 °C for 4 hours in order to remove any moisture and then ground to < 100 mesh (0.15mm) with a pulverizer. **Table 1** shows the EMR chemical composition. As can be seen, ammonium sulfate ($(NH_4)_2SO_4$) is one of the major components in the EMR as it forms nearly 13 wt.%, whereas Mn makes up only about 5 wt.%. A more analysis of the manganese-containing phases are detailed in **Table 2**. These findings show the presence of a number of Mn compounds that include the main phases $MnCO_3$ and $MnSO_4$ – that account for > 95% of the total sample manganese content - as well as minor levels of $MnSiO_3$ and MnO_2. The presence of $MnCO_3$ and $MnSiO_3$ results from the non-leached part of the original ores (Zhang and Cheng, 2007), whilst $MnSO_4$ originate from the leaching process (Shu et al., 2016b; Shu et al., 2016c; Shu et al., 2018a; Shu et al., 2019a) and MnO_2 comes from unreacted pyrolusite in the ferrous ion oxidization stage (Xu et al., 2014; Brantley and Rampacek, 1968; Duan et al., 2011).

XRD and SEM analysis showed EMR to be a black powder made up of irregularly

shaped agglomerate particles that contained mainly quartz (SiO_2), pyrite (FeS_2), rhodochrosite ($MnCO_3$), magnesite ($MgCO_3$), gypsum ($CaSO_4 \cdot 2H_2O$), and muscovite ($K(Na)_2O \cdot Al_2O_3 \cdot SiO_2$) (**Fig. 1(a)** and **(b)**). Additionally, EDS mapping of the material is shown in **Fig. 1(c)** and this clearly indicates the coincidental distribution of Si and O, which when combined with the XRD pattern (**Fig. 1(a)**), highlights the presence of an independent quartz ore phase. It was found that the distributions of Si, O, Al, K (Na) as well as Fe, S were also similar, which indicated that the EMR also contained both muscovite and pyrite ore phases. In contrast, Ca and Mn were randomly distributed throughout the whole analysis area.

Table 1 Chemical composition of the EMR investigated.

Element	Al	Ti	Ca	S	Na	Fe	K	Mg	Mn
Content (wt.%)	4.83	0.33	5.33	9.29	0.63	5.26	1.60	1.63	4.57
Element	Ba	Ni	Pb	Cr	Cu	Zn	Si	$(NH_4)_2SO_4$	
Content (wt.%)	0.05	0.01	0.02	0.01	0.01	0.01	24.82	12.89	

Table 2 Manganese-containing phases identified within EMR.

Mn containing Phase	$MnCO_3$	$MnSO_4$	$MnSiO_3$	MnO_2	Total
Mn Content (wt.%)	2.77	1.59	0.14	0.07	4.57
Phase occupation ratio (%)	60.63	34.79	3.05	1.53	100

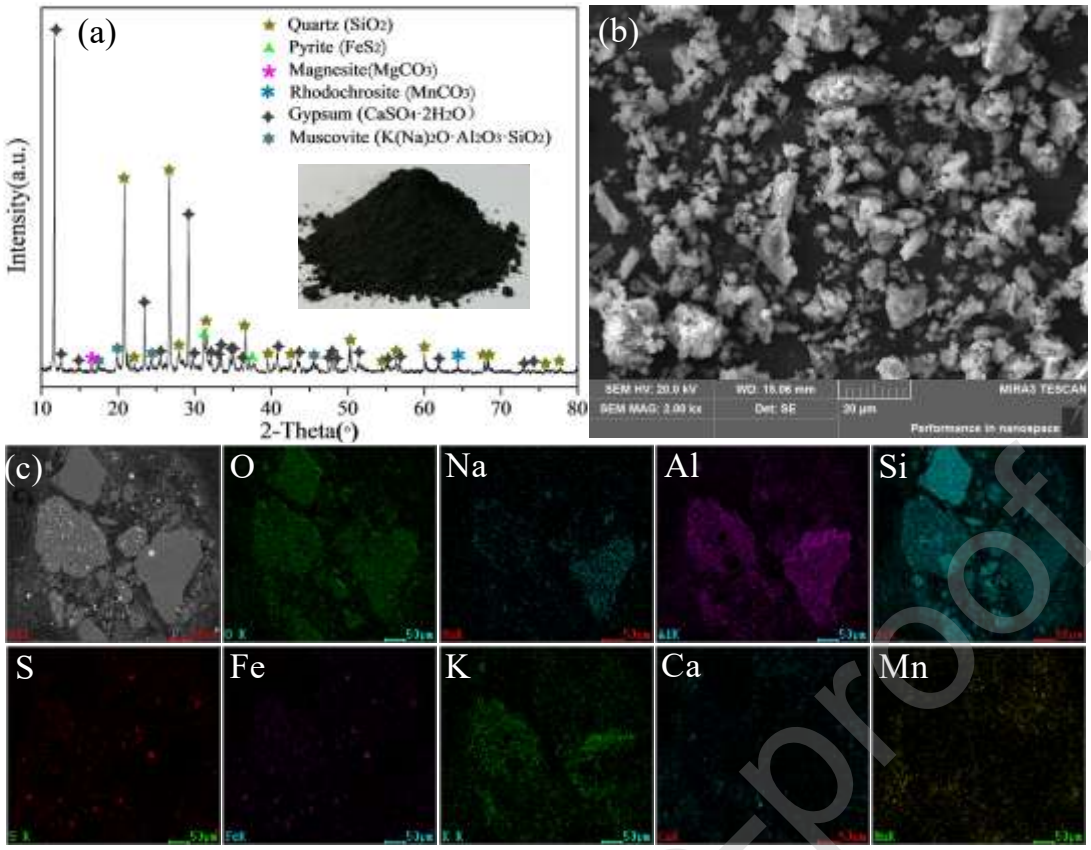

Fig.1 Characterization of the EMR sample: (a) General appearance and XRD pattern, (b) SEM morphology and (c) EDS mapping scanning images

2.2 Low temperature roasting

A predetermined amount of the EMR sample was weighed into a flat bottom crucible, before it was placed in a muffle furnace at the desired roasting temperature. Roasting was performed in the presence of a controlled airflow, with any flue-gas produced absorbed and treated by an integrated flue gas recovery system. Roasting temperature was varied between 450 and 650 °C, whilst the roasting time were separately investigated from 30 to 120 min, and the samples roasted in different conditions were marked as $R_{time/temperature}$. After roasting, samples were removed from the muffle furnace, cooled in air and weighed prior to subsequent analysis, whilst the quality change and roasting loss rate of EMR sample before and after roasting in different condition as outlined in **Supplementary Table 1**.

2.3 Water washing

Water-washing experiments were carried out using a mixture of EMR or roasted EMR and deionized water with a solid-liquid ratio of 1:4 (g/ml) sample that was placed in a beaker with stirring and heated by a water bath to 25 °C (manganese sulfate has the highest solubility in 25°C water under normal pressure (Haynes et al., 2015)). In the case of the washing-time experiments, a 5ml slurry was collected at regular washing time intervals and then centrifuged in order to obtain a supernatant for ICP Mn concentration analysis. For all other water-washing experiments the slurry was washed for 30 min, then filtrated by a sand core filter, before the filter residues were oven-dried at 105 °C for 4 h. The volume of washing solution was recorded and the Mn solution concentration was determined by ICP. The recovery ratio of Mn in the washing solution was calculated using the following formula:

$$\alpha = \frac{C_{Mn} \times V_L}{m_D \times W_{Mn}} \times 100\%$$

where α is the recovery ratio of manganese from EMR, %; C_{Mn}, the manganese concentration in the washing solution in g/L; V_L, volume of the washing solution in L, m_D, the mass of EMR used for the washing in g and W_{Mn}, the EMR sample mass Mn percentage used in the washing in wt.%.

2.4 Toxicity leaching

Toxicity leaching experiments for the untreated and the treated EMRs were carried out according to the HJ/T 300-2007 (Standards, 2007). The toxicity was evaluated by comparison of the ion concentrations in the leaching solution with the regulatory limits of the GB 8978-1996 (Standards, 1996).

2.5 Analysis methods

Photos that show the macro scale appearance of the samples were taken by a mobile phone camera (Samsung, Note 8). The phases of the as-received and roasted EMR samples were identified using X-ray diffraction analysis (XRD, Rigaku, TTR- III, Cu target, Kα1, λ = 0.15406 nm). Micro-morphological and elemental mapping analyses were conducted with a field emission scanning electron microscope (SEM, TESCAN, MIRA3 LMU) equipped with an energy-dispersive spectrometer (EDS, EDAX, Oxford X-Max20). The Low temperature roasting characteristics of EMR was determined by a simultaneous thermal analyzer (TG-DSC, SDTQ600, TA instruments) over a temperature range of 25 to 1000 °C in an air atmosphere, using a heating rate of 10 °C/min. Characteristic vibration peaks of the materials were measured by a Fourier Transform Infrared spectrometer (FT-IR, Thermo Fisher, Nicolet 6700, 32 scans, Resolution: 4 cm^{-1}) using disc samples prepared with KBr.

Ammonium sulfate content of the EMR samples was determined according to the analysis method of GB 535-1995 (Standards, 1995). Levels of Cr^{6+} in the toxicity leaching solutions was determined via the analysis method of HJ 908-2017 (Standards, 2017), and the CN^- determination within the same solutions followed the methodology outlined in HJ 484-2009 (Standards, 2009a). In addition, toxicity leaching solution NH_4^+-N and F^- contents were ascertained according to HJ 535-2009 (Standards, 2009b) and GB/T 205-2000 (Standards, 2000). Amounts of the remaining elements in solid samples and leaching solutions were determined by ICP-AES analysis (ICP, Thermo Scientific, iCAP 7000).

3. Results and discussion

3.1 Experimental mechanism

One of the main objectives of this study was to investigate the phase transformation characteristics of the EMR sample under low temperature roasting conditions in air. During the low temperature roasting process, the following reactions are possible:

$CaSO_4 \cdot 2H_2O(s) \rightarrow CaSO_4 \cdot 0.5H_2O(s) + 1.5H_2O(g)$ (1)

$CaSO_4 \cdot 0.5H_2O(s) \rightarrow CaSO_4(s) + 0.5H_2O(g)$ (2)

$CaSO_4 \cdot 2H_2O(s) \rightarrow CaSO_4(s) + 2H_2O(g)$ (3)

$MgCO_3(s) \rightarrow MgO(s) + CO_2(g)$ (4)

$MgO(s) + SO_2(g) + 0.5O_2(g) \rightarrow MgSO_4(s)$ (5)

$MgCO_3(s) + SO_2(g) + 0.5O_2(g) \rightarrow MgSO_4(s) + CO_2(g)$ (6)

$MgCO_3(s) + (NH_4)_2SO_4(s) \rightarrow MgSO_4(s) + 2NH_3(g) + CO_2(g) + H_2O(g)$ (7)

$FeS_2(s) + 5.5O_2(g) \rightarrow 0.5\ Fe_2O_3(s) + 2\ SO_2(g)$ (8)

$MnCO_3(s) \rightarrow MnO(s) + CO_2(g)$ (9)

$MnO(s) + SO_2(g) + 0.5O_2(g) \rightarrow MnSO_4(s)$ (10)

$MnCO_3(s) + SO_2(g) + 0.5O_2(g) \rightarrow MnSO_4(s) + CO_2(g)$ (11)

$MnCO_3(s) + (NH_4)_2SO_4(s) \rightarrow MnSO_4(s) + 2NH_3(g) + CO_2(g) + H_2O(g)$ (12)

$(NH_4)_2SO_4(s) \rightarrow 2NH_3(g) + SO_2(g) + H_2O(g) + 0.5O_2(g)$ (13)

The HSC Chemistry 9.0 (HSC Chemistry, 2019) was used to calculate the reaction equilibrium of phase transformation during roasting process with Gibbs free energy minimization under isothermal, isobaric and unit mole target reactant - such as, $CaSO_4 \cdot 2H_2O(s)$, $MgCO_3(s)$, $FeS_2(s)$, $MnCO_3(s)$, $(NH_4)_2SO_4(s)$ - conditions. **Fig. 2 (a, b)** shows the standard Gibbs free energy changes of the chemical reactions (Eq. 1 - 13) over a temperature range of 25 - 650 °C. Eq. (1 - 3) outlines the well-known stepwise gypsum dehydration reaction (Engbrecht and Hirschfeld, 2016; Yang et al., 2018) and as can be seen from **Fig.2(a)**, the standard Gibbs free energy of these equations (Eq. (1 - 3)**)** becomes increasingly negative as temperature is elevated above 100 °C, which indicates a greater reaction tendency. Eq. (4 - 7) relate to the phase transformation reactions of magnesite - e.g. decomposition and sulfonation (Sadik et al., 2016) - which, according to **Fig. 2(a)**, occur above 430 °C (Eq. (4)) and at > 250 °C (Eq. (7)) and this indicates that the reaction of Eq.(7) is the more likely *cf.* **(**Eq. (4)) in the low temperature roasting process.

In **Fig. 2(b)** the standard Gibbs free energy of Eq. (5) and (6) are negative across a temperature range from 25 - 650 °C and within this range, the reaction trend is more

pronounced than that determined for Eq. (4) and (7). In addition, the pyrite phase transformation/oxidation reaction (Yang et al., 2009; Jassim et al., 2011) outlined in Eq. (8) was found to possess a significantly negative standard Gibbs free energy over the same temperature range (**Fig. 2(b)**) highlighting the extremely facile nature of the reaction. In contrast, the rhodochrosite phase transformation, decomposition and sulfonation (Chen et al., 2016) reaction steps shown in **Fig. 2(a)** (Eq. (9-12)) can only occur either at > 190 °C, like Eq. (12) or > 340 °C (Eq. (9)), though with low-temperature roasting Eq. (12) is thermodynamically more likely. On the other hand, although the calculated free energy of Eq. (10) and (11) displayed in **Fig. 2b** are also negative between 25 - 650 °C, the reaction trends are more pronounced than that determined for Eq. (9) and (12). Conversely, the direct decomposition reaction of ammonium sulfate (Mohamed et al., 2016) - shown in Eq. (13) – only reaches a negative standard Gibbs free energy above 525 °C. Nevertheless, based on the thermodynamic calculations and the possible chemical reaction series although direct ammonium sulfate decomposition only occurs at temperature > 525 °C, the other reactions - Eq. (1)-(12) - that can facilitate the effective decomposition of ammonium sulfate all occur at temperatures of < 430 °C.

The TG-DSC curve of EMR over a temperature range of 25 - 1000 °C is displayed in **Fig. 2(c)**. As can be seen from the measurement, the EMR sample starts to lose weight from around 70 °C as gypsum dehydration commences in line with Eq. (1) (Dolezělová et al., 2018). With the continued elevation in temperature ≤ 200 °C, further weight loss is detected as first the initial gypsum dehydration is completed – signified by the small heat absorption peak at 108 °C (Engbrecht and Hirschfeld, 2016) – then the conversion of $CaSO_4 \cdot 2H_2O(s)$ to $CaSO_4(s)$ (Iucolano et al., 2018) (Eq. (2)) that results in a 2.9 wt.% decrease. When the temperature reaches 210 °C $(NH_4)_2SO_4(s)$ begins to melt (Li et al., 2017), which initiates the change of $MnCO_3(s)$, $MgCO_3(s)$, $(NH_4)_2SO_4(s)$ to $MnSO_4(s)$, $MgSO_4(s)$ and flue gases $NH_3(g)$, $CO_2(g)$, $H_2O(g)$ following the reactions outlined in Eq. (7) to (12) that give rise to a further 2.1 wt.% loss by the time the temperature is 430 °C (Sadik et al., 2016). Above 445 °C, pyrite ($FeS_2(s)$) begins to decompose and

oxidize as shown by the initiation of a clear exothermic peak at 490 °C (Huang et al., 2015). This chemical reaction (Eq. (8)) is complete once the DSC curve reaches 610 °C and the associated weight reduction was determined to be 3.2 wt.%.

As the temperature increases > 650 °C, some of the sulfates present in the material ($MnSO_4$(s), $MgSO_4$(s), etc.) begin to melt and decompose (Mao et al., 2011), which leads to the formation of higher valence manganese compounds as well as complex composite minerals through combination with MgO and/or other elements present in the material. Therefore, in order to realize the complete decomposition of ammonium sulfate in EMR, and transformation of the rhodochrosite into soluble $MnSO_4$, low temperature roasting between 450 and 650 °C is preferable. In addition, under the same conditions, pyrite is converted into more stable and environmentally inert, hematite. If the roasting temperature exceeds 650 °C, manganese sulfate is further converted into water insoluble manganese oxides (Mao et al., 2011), which cannot be recovered via water-leaching.

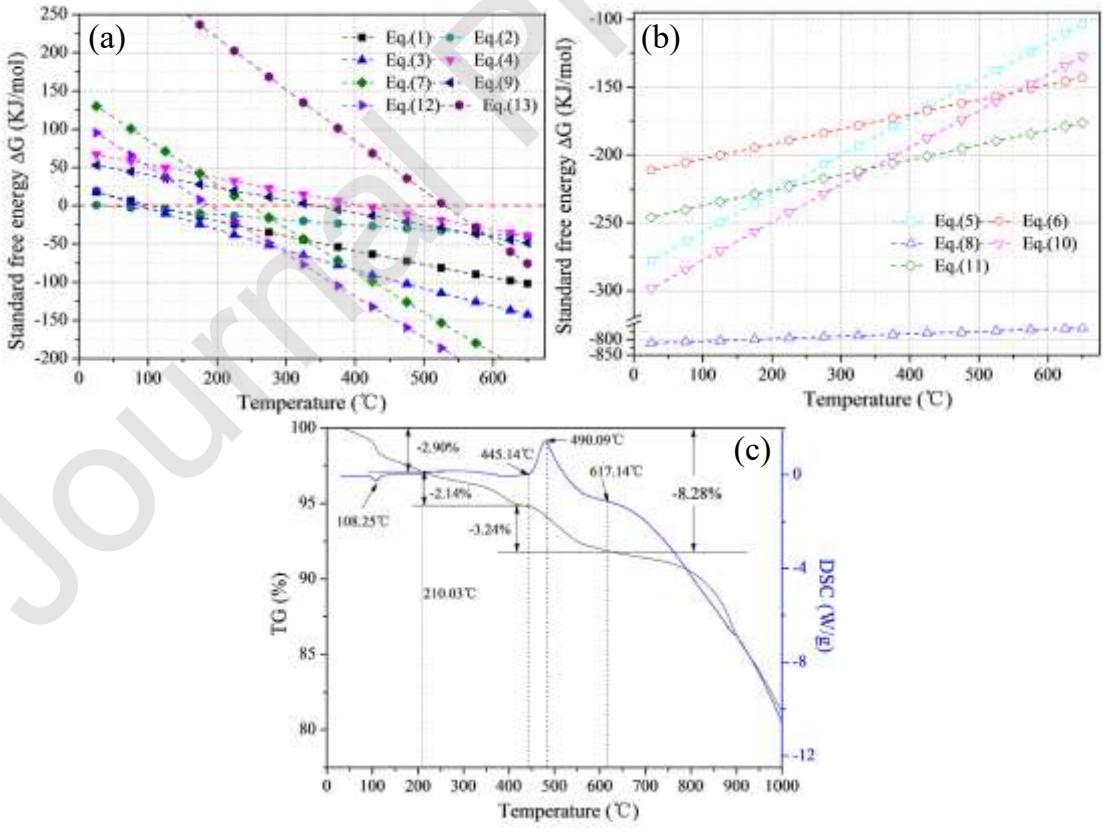

Fig. 2 The low-temperature roasting reaction mechanism of the EMR sample under air atmosphere: (a), (b) standard Gibbs free energy change of Eq. (1)-(13) in the temperature range of 25-650 °C and (c) the TG-DSC curve of EMR in the temperature range of 25-1000 °C under an air atmosphere.

3.2 Effect of roasting temperature

The effect of roasting temperature on the chemical composition of EMR samples was investigated after roasting in air for 120 min at temperatures between 450 - 650 °C and the related XRD sample pattern are displayed in **Fig. 3**. As can be seen, the characteristic peaks of gypsum ($CaSO_4 \cdot 2H_2O$), magnesite ($MgCO_3$), rhodochrosite ($MnCO_3$) and pyrite (FeS_2) all present in the initial raw material disappear during roasting and are replaced by peaks associated with calcium sulfate ($CaSO_4$) and hematite (Fe_2O_3).The changes indicate that gypsum, magnesite, rhodochrosite and pyrite (FeS_2) all undergo phase transformations as a result of heating; gypsum in particular, changes to anhydrous calcium sulfate through the loss of moisture. At the same time, pyrite (FeS_2) is oxidized into hematite and as roasting temperature is increased, the diffraction intensity of the characteristic hematite peaks are enhanced demonstrating that higher roasting temperatures promote pyrite transformation. In contrast, the results also show that there was no significant change in the diffraction peak related to muscovite ($K(Na)_2O \cdot Al_2O_3 \cdot SiO_2$).

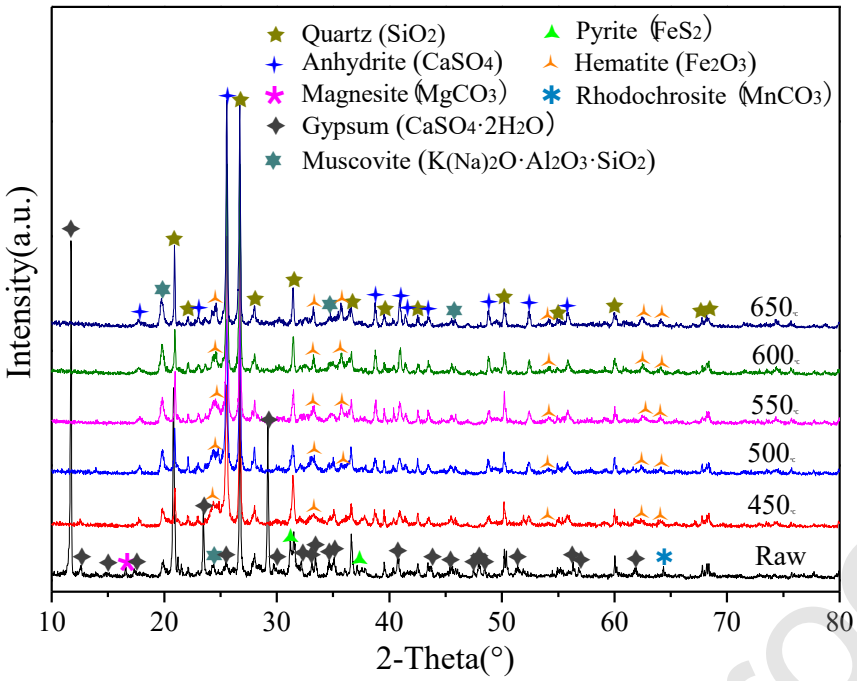

Fig. 3 XRD patterns of roasted EMR samples at different roasting temperatures.

Fig. 4 displays the FT-IR spectra for EMR samples roasted in air for 120 min between 450 and 650 °C. These results show that unroasted EMR samples have a spectral band centered around ~3600 cm^{-1} that corresponds to the strong O-H bond stretching vibrations of crystalline water (Shen et al., 2017). The band at 1432 cm^{-1} is related to the -NH_4^+ vibration band of $(NH_4)_2SO_4$ (Cai et al., 2017), Fe-S stretching of pyrite is observed at 1094 cm^{-1} (Middya et al., 2014), whereas the bands at 600 and 530 cm^{-1} corresponds with pyrite S-S stretching vibrations (Bemana and Nadimi, 2017). When samples are roasted, the spectral vibration bands in the regions of 622 and 595 cm^{-1} appear, which are indicative of Fe-O stretching and bending peaks related to Hematite (Philias and Marsan, 1999; Jing and Wu, 2004; Yan and Zhang, 2011). Moreover, the O-H vibration band at 3554 cm^{-1} disappears as EMR is heated up to 650°C, suggesting the loss of the crystalline waters of gypsum phase as outlined in Eq. (1)-(3). Similarly, the -OH vibration peak of crystalline water centered around 3600 cm^{-1} is also observed to have disappeared, which suggests that crystalline water is also removed from the other minerals present. Additionally, the -NH_4^+ vibration around 1431cm^{-1} is also found to be absent once the roasting temperature reaches 500 °C showing that ammonium

sulfate in the samples becomes completely decomposed in line with one or more of the reactions outlined in Eq. (7), (8), (13). Once the roasting temperature reached > 550 °C, the Fe-S vibration band (1094 cm^{-1}) and the S-S vibrations (at 600 and 530 cm^{-1}) cease to be visible demonstrating that the pyrite phase present in the raw material undergoes transformation to hematite (Eq. 8). This is confirmed by the gradual appearance of clear Fe-O vibration bands around 622 and 595 cm^{-1} with increased roasting temperatures.

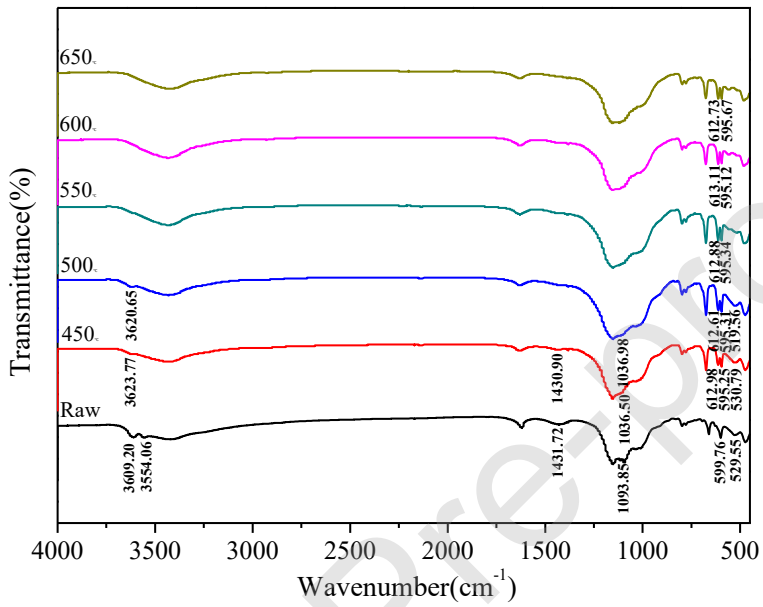

Fig. 4 FT-IR spectral curves of EMR samples roasted at different temperatures.

According to the EDS mapping analysis in **Fig. 1(c)**, the EMR contains an independent pyrite ore phase. **Fig. 5** displays the macroscale appearances and EDS mapping for EMR samples roasted in air for 120 min at temperatures between 450 and 650 °C. These results show that the colors of roasted EMRs changed from black to dark red as roasting temperature was increased. The distributions of Fe and S elements in $R_{120\ min/450\ °C}$ are generally coincident (**Fig. 5(b)**) and is similar to the observations with the EMR raw material (**Fig. 5(a)**), indicating that the oxidation rate of pyrite is slower at 450 °C. The distributions of O, S and Fe elements in $R_{120min/500\ °C}$ are also correlated, as the distributions of O and Fe elements are coincident at the outer interface, whereas S and Fe are clearly associated at the inner interface. The results show that the pyrite in EMR was gradually oxidized from the outside of the particle with only partial pyrite oxidation

to hematite occurred with roasting 120 min at 500 °C. In contrast, when temperatures are ≥ 550 °C, there is no significant overlap of the distribution of S and Fe elements in roasted EMR, and the distribution of O, Fe elements in the roasted EMR are fully coincident (**Fig. 5(d-f)**), which clear suggests that that the pyrite phase was completely converted to hematite. From a comprehensive analysis of the results in **Fig 3, 4** and **5**, it can be concluded that the unstable phases of gypsum ($CaSO_4 \cdot 2H_2O$), magnesite ($MgCO_3$), rhodochrosite ($MnCO_3$), ammonium sulfate ($(NH_4)_2SO_4$) and pyrite (FeS_2) present in EMR can be completely converted into more stable phases with a roasting treatment at temperatures of 550 °C or higher after 120 min.

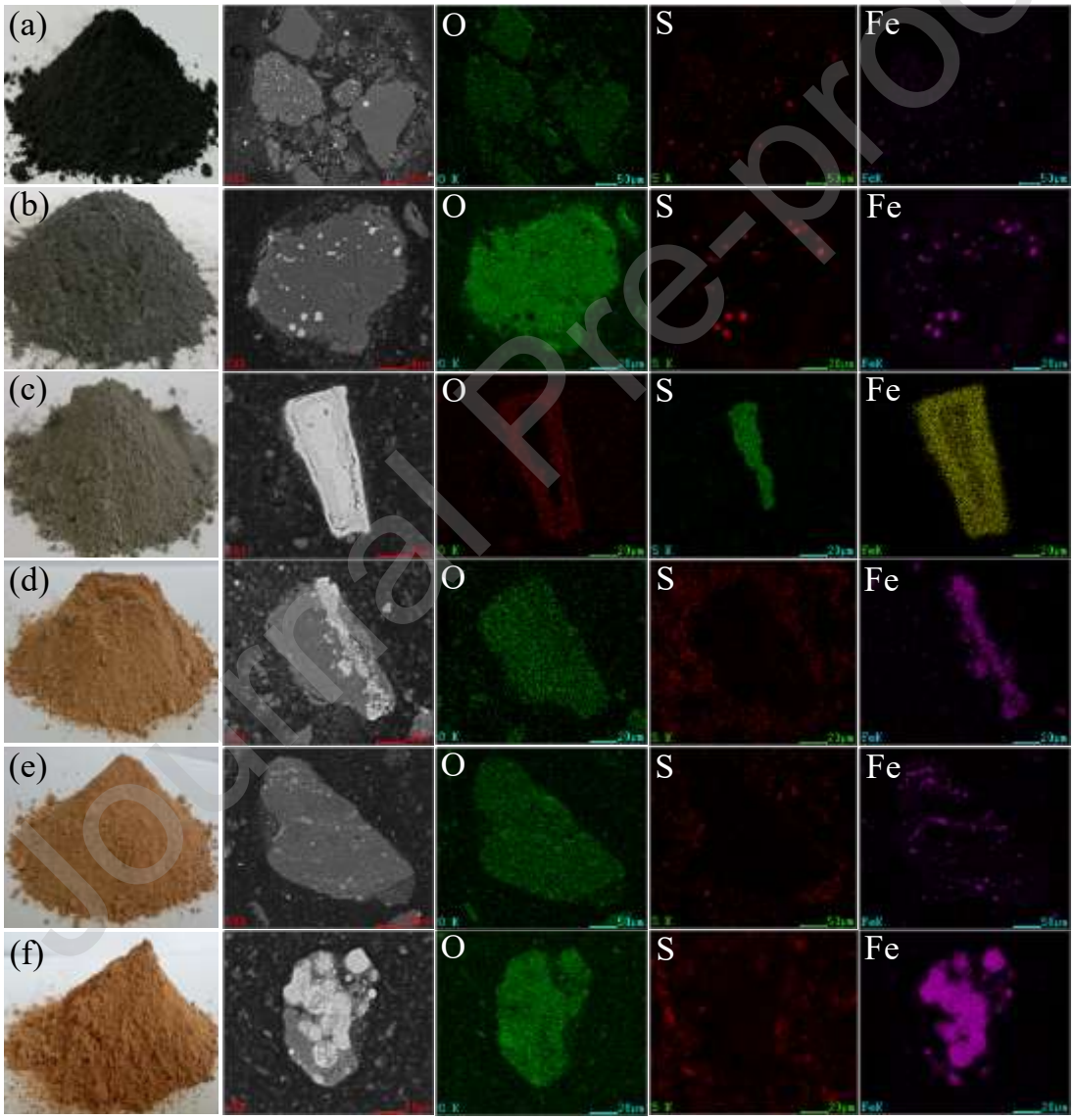

Fig. 5 The appearance photos of EMR samples and mapping scanning images results of the

transformation characteristics of their pyrite phases at different temperatures: (a) the EMR sample; (b) $R_{120min/450\ °C}$; (c) $R_{120min/500\ °C}$; (d) $R_{120min/550°C}$; (e) $R_{120min/600°C}$; (f) $R_{120min/650\ °C}$

3.3 Effect of roasting time

The effect of roasting time was further investigated on the phase conversions by variation of the roasting time duration between 30 to 120 min temperatures between 550 to 650 °C. The chemical composition and related XRD sample patterns are displayed in **Fig. 6(a-c)**. As can be seen, the characteristic peaks of gypsum ($CaSO_4 \cdot 2H_2O$), magnesite ($MgCO_3$), rhodochrosite ($MnCO_3$) and pyrite (FeS_2) all present in the initial raw material, clearly disappear during roasting and are replaced by patterns associated with calcium sulfate ($CaSO_4$) and hematite (Fe_2O_3) for all times and temperatures investigated.

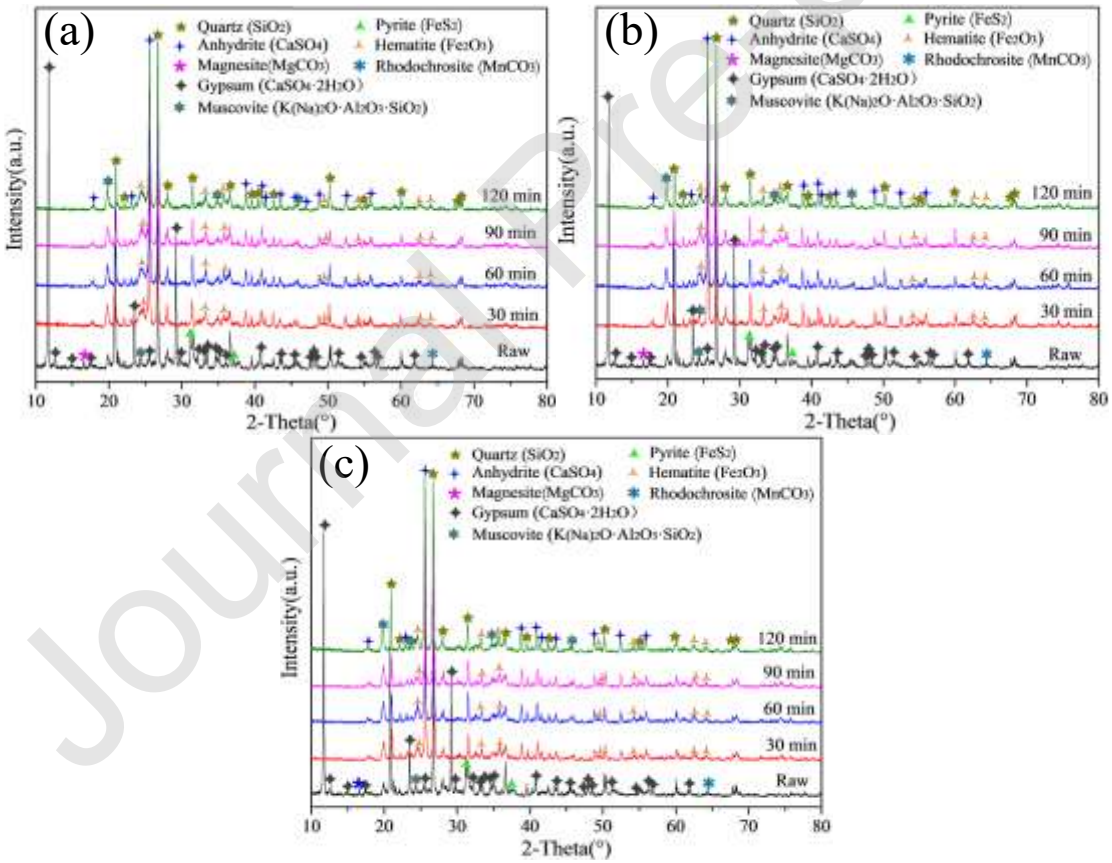

Fig. 6 The XRD patterns of roasted EMR samples for different roasting time at different roasting temperatures: (a) 550 °C; (b) 600 °C; (c) 650 °C

Fig. 7 displays the FT-IR spectra for EMR samples roasted in air from 30 to 120 min at temperatures between 550 to 650 °C. These results show that the strong O-H bond stretching vibrations related to crystalline water around 3609 cm^{-1}, the $-NH_4^+$ vibration band at 1432cm^{-1}, Fe-S stretching of pyrite is observed at 1094 cm^{-1}, and the bands at 600 and 530 cm^{-1} related with pyrite S-S stretching vibrations all disappear after roasting for more than 30 minutes at temperatures ≥ 550 to 650 °C. In contrast to the disappearance of these bands, spectral vibration bands in the regions of 622 and 595 cm^{-1} related to Fe-O appear at the same time. These results show that complete gypsum dehydration is achieved, the ammonium sulfate present decomposes/transforms and pyrite oxidizes into hematite at temperature ≥ 550 °C and times of 30 min or longer.

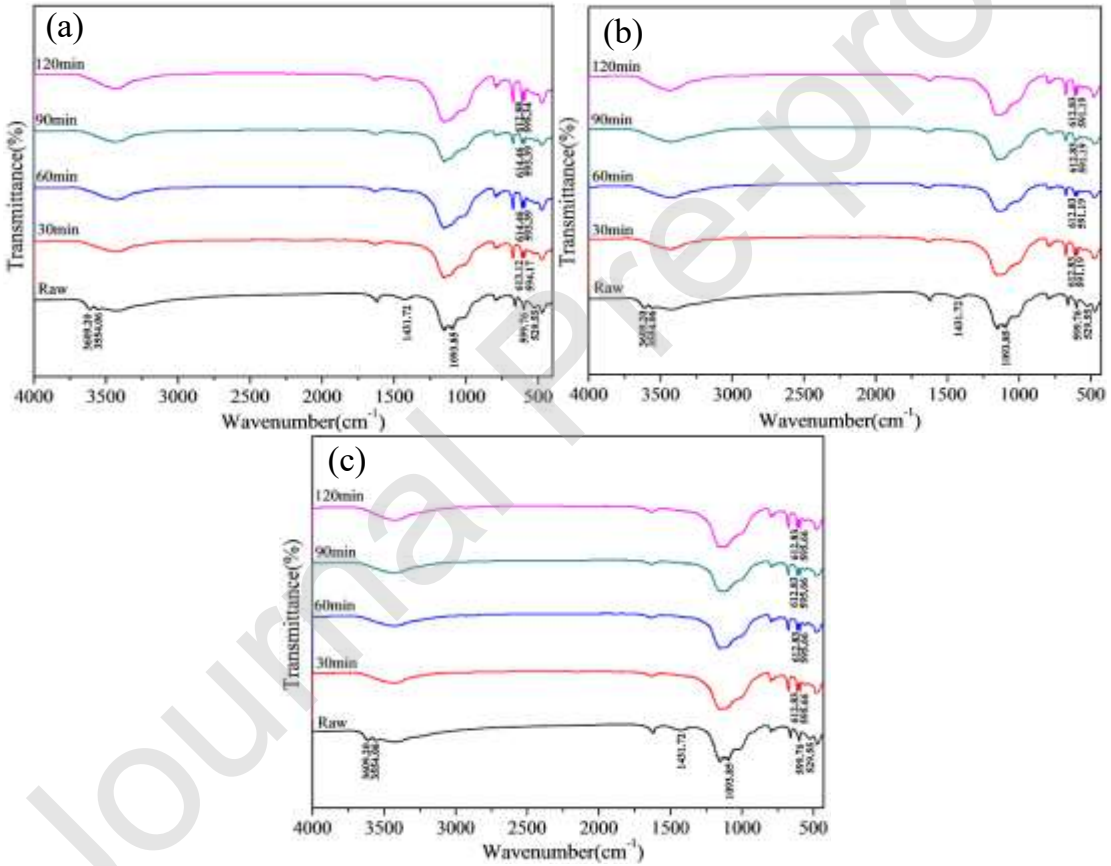

Fig.7 FT-IR spectral curves of EMR samples roasted for different roasting time at different temperatures: (a) 550 °C; (b) 600 °C; (c) 650 °C

As the pyrite phase is completely converted to hematite phase after 120 min roasting above 550 °C (**Fig. 5)**, the effect of roasting time on pyrite phase transformation at

temperatures of 550 °C and above was investigated. The macroscale appearances and EDS mapping for EMR samples roasted in air from 30 to 120 min at temperatures between 550 to 650 °C are displayed in **Fig. 8**. These results show that the colors of roasted EMR changed from dark red to khaki as roasting time was increased from 30 to 120 min at 550 °C. This color change could be explained by the reductions in Fe and S distributions within the material as a result of pyrite conversion to hematite during the roasting, is complete after 120 min at 550 °C (**Fig. 8-I**). Roasting of EMR at 600 °C for 30 to 60 min results in a crimson color, however analysis of the resulting materials indicate that there is no correlation between the distributions of Fe and S signifying that completely hematite conversion occurs within 60 min of roasting at 600 °C (**Fig. 8-II**). In contrast, EMR material roasted for 30 min at 650 °C is khaki in color, similar to that observed for $R_{120min/550°C}$. As was found with roasting at 600 °C, the distributions of S and Fe elements also did not correlate, which means the pyrite was completely converted to hematite already within 30 min at 650 °C (**Fig. 8-III**). From these results, it is concluded that the unstable phases of gypsum ($CaSO_4 \cdot 2H_2O$), magnesite ($MgCO_3$), rhodochrosite ($MnCO_3$), ammonium sulfate ($(NH_4)_2SO_4$) and pyrite (FeS_2) present in EMR can be completely converted into more stable phases with the following roasting parameters: 120min at 550 °C; 60min at 600 °C; and 30min at 650 °C.

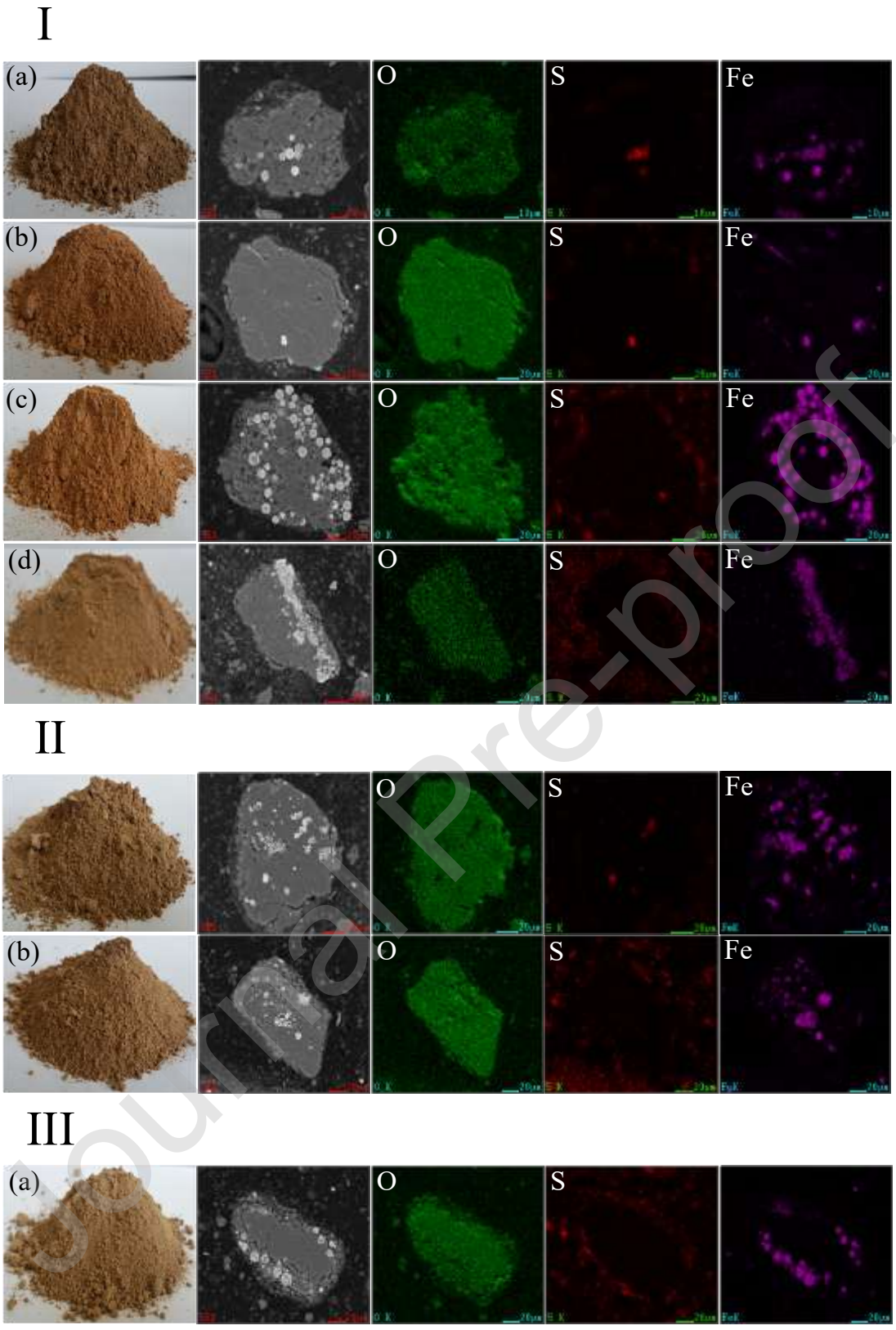

Fig. 8. Appearance of EMR and EDS mapping of the pyrite transformation characteristics for different roasting times at temperatures of: **I** 550 °C (a) 30 min, (b) 60min, (c)90min, (d)120min; **II** 600 °C (a)30min, (b)60min; **III** 650 °C: (a) 30min.

3.4 Water-washing properties of manganese within roasted EMR

Based on the results from the previous experiments of roasting temperature and time on the phase transformation in EMR, the water-leaching properties of manganese in roasted EMRs were investigated and the results are shown in **Fig. 9**. The recovery rate of manganese from samples roasted at 550 °C increased slightly with longer roasting times and the maximum Mn recovery achieved was 65.66 % with 120 min of roasting. At 600 °C, Mn recovery was found to increase initially before reducing with extended roasting durations with a maximum recovery of 67.12 % for Mn found after 60 min heat treatment. In contrast, Mn recovery rates from samples roasted at 650 °C decreased gradually with the increased of roasting time, and the highest recovery rate was 48.19 % after 30 min.

Based on these results it is evident that higher roasting temperatures are not conducive to recovering the Mn in EMR by the water-washing method, as Mn recovery rates were significantly higher at both 550 °C and 600 °C, when compared to that achieved at 650 °C. Furthermore, recovery rates of Mn from samples roasted at 600 °C and 650 °C were also seen to decrease markedly when the roasting time exceeds 60 min, which indicates that the extended roasting times are also not beneficial for enhanced Mn recovery from EMR materials. From the results it can be deduced that 60 min roasting at 600 °C ($R_{60min/600°C}$) provided the highest Mn recovery rate (~ 67.12 %).

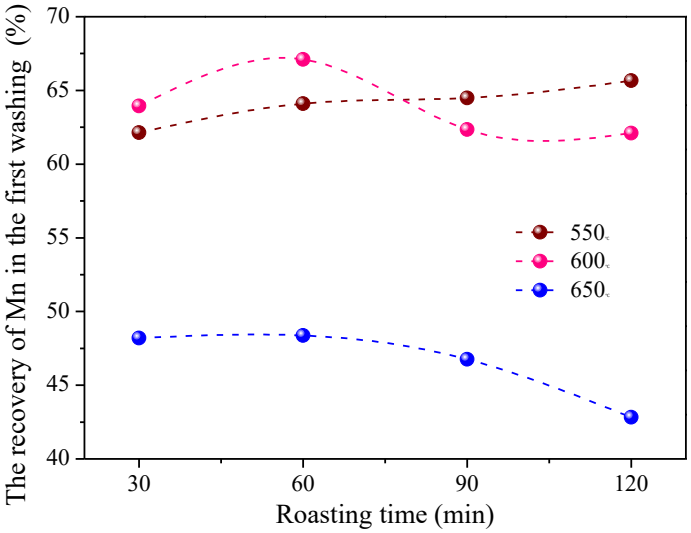

Fig. 9 Recovery rate of manganese from EMR roasted at different temperatures and durations in the first water-washing process.

As a consequence of the initial results related to roasting temperature and duration the effect of washing time on the Mn recovery rate of manganese from roasted EMR was investigated. As can be seen from **Table 3**, prolonged washing times had only a marginal effect on the overall rate of Mn recovery and that a maximum recovery of ~ 67 % was found after 25 min of washing, a time that was subsequently selected for the following experiments. $R_{60min/600°C}$ was washed sequentially with deionized water and the results are shown in **Table 4**. From the results it can be seen that the content of Mn in the 1st washing solution is 16.88 g/L and this reduces significantly with each subsequent wash cycle until a level of less than 0.005 g/L is achieved after the sixth wash. These findings indicate that the soluble Mn in $R_{60min/600°C}$ can be almost completely removed after 6 separate washing stages. On the other hand, when the roasted EMR material $R_{60min/600°C}$ washer water was recirculated to the next washing stage a continuous enrichment in Mn was observed as shown in **Table 5**. The results demonstrate that the content of manganese in the washing solution reaches 40.12 g/L after only the third circulation and this concentration is consummate with the level required for electrolytic metal manganese production of about 40 g/L (Mei et al., 2011).

Table 3 Effect of washing time on the primary washing recovery rate of manganese in $R_{60min/600°C}$.

Washing Time (min)	5	10	15	20	25	30	40	50	60
Efficiency (%)	64.15	64.38	66.58	66.92	67.37	67.12	67.56	67.52	67.45

Table 4 Manganese content in solution from $R_{60min/600°C}$ sequentially washed with deionized water.

Washing Times	1st	2nd	3rd	4th	5th	6th
Mn^{2+} Concentration (g/L)	16.88	5.03	1.11	0.22	0.04	＜0.005

Table 5 Enrichment of the manganese content in the recirculated washing water solution from the treatment of $R_{60min/600°C.}$

Enrichment Times	1	2	3	4	5	6
Mn^{2+} Concentration (g/L)	16.88	29.09	40.12	50.78	57.74	61.56

3.5 The toxic leaching properties of the treated EMR sample

As EMR is an environmental hazard, toxicity leaching tests were carried out to determine the leaching characteristics before and after the roasting treatment process (**Table 6)**. The finding in **Table 6** show that the NH_4^+-N content in the leaching solution of the untreated EMR sample reaches 273.62 mg/L, which is over 10 times higher than that of the standard limit value 25.00 mg/L. In contrast, the leaching solution of EMR treated by the roasting – water washing process has an NH_4^+-N content of 0 mg/L, which indicates the successful removal of NH_4^+-N from the EMR sample. The concentration of Mn in the leach solution was also reduced from the untreated 859.10 mg/L to the treated 1.30 mg/L which is also lower than the standard limit 2.00 mg/L. In the case of Cu, the level in the untreated EMR sample is equivalent to the standard limit value of 2 mg/L, whereas this is reduced to 0.2mg/L after treatment. Similar reductions after treatment to below the acceptable limits of the GB 8978-1996 standard are also found for Be (0.008 mg/L to the 0.003 mg/L), Ni (1.4 mg/L to 0.05 mg/L) which is lower than the standard limit 1.00 mg/L. Furthermore, although the concentrations of Pb, ※T_{Cr}, Zn, Ba, As, Se and F^-in the untreated EMR leaching solution are all lower than the GB 8978-1996 limit, these concentrations are further reduced after treatment and clearly highlight the beneficial effects that the low-temperature roasting and water

washing treatment can achieve for towards the aim of hazard-free stockpiling of EMR wastes.

Table 6. Comparison of the leaching characteristics of untreated and treated EMR materials.

Elements	Raw(mg/L)	Treated residue(mg/L)	GB8978-1996 (mg/L)
Hg	-	-	0.05
NH_4^+/N	273.62	-	25.00
Pb	0.08	0.06	1.00
Cd	0.03	0.03	0.10
※T_{Cr}	0.02	0.01	1.50
Cr^{6+}	-	-	0.05
Cu	2.00	0.20	2.00
Zn	1.00	0.20	2.00
Be	0.008	0.003	0.005
Ba	0.09	0.06	-
Ni	1.40	0.05	1.00
Ag	-	-	0.50
As	0.40	0.10	0.50
Se	0.04	0.01	0.50
Mn	859.10	1.30	2.00
F^-	4.48	4.38	20.00
CN^-	-	-	1.00

Note: ※T_{Cr} represents the total Cr in the toxic leaching solution.

Based on all the analysis results, EMR can be readily treated by the low temperature roasting – water washing process, to produce a Mn solution that can be recycled and an innocuous EMR residue that can be safely stockpiled via process flowsheet shown in **Fig. 10**. The electrolytic manganese residue collected by a slag dump is dried and crushed into EMR powder particles with certain granularity. Then a continuous-working roasting equipment, such as rotary kiln, is used to roast the EMR powder particles for 60 min at 600 °C. Flue gases of NH_3(g) and SO_2(g) produced during the process are collected by the flue gas recovery system and reused in the acid leaching of electrolytic manganese production. The roasted EMR is cooled down with an air-cooling device. The high temperature air generated during the cooling process is used in the waste heat boiler which produces the high temperature steam for the drying process of EMR (Luo et al., 2017). In the end, the roasted EMR is countercurrent water-

washed, which generates both of the hazard-free EMR and manganese-containing washing solution. The manganese-containing washing solution meets the process requirements of electrolytic manganese metal production; therefore, it can return to the manganese metal electrolysis process.

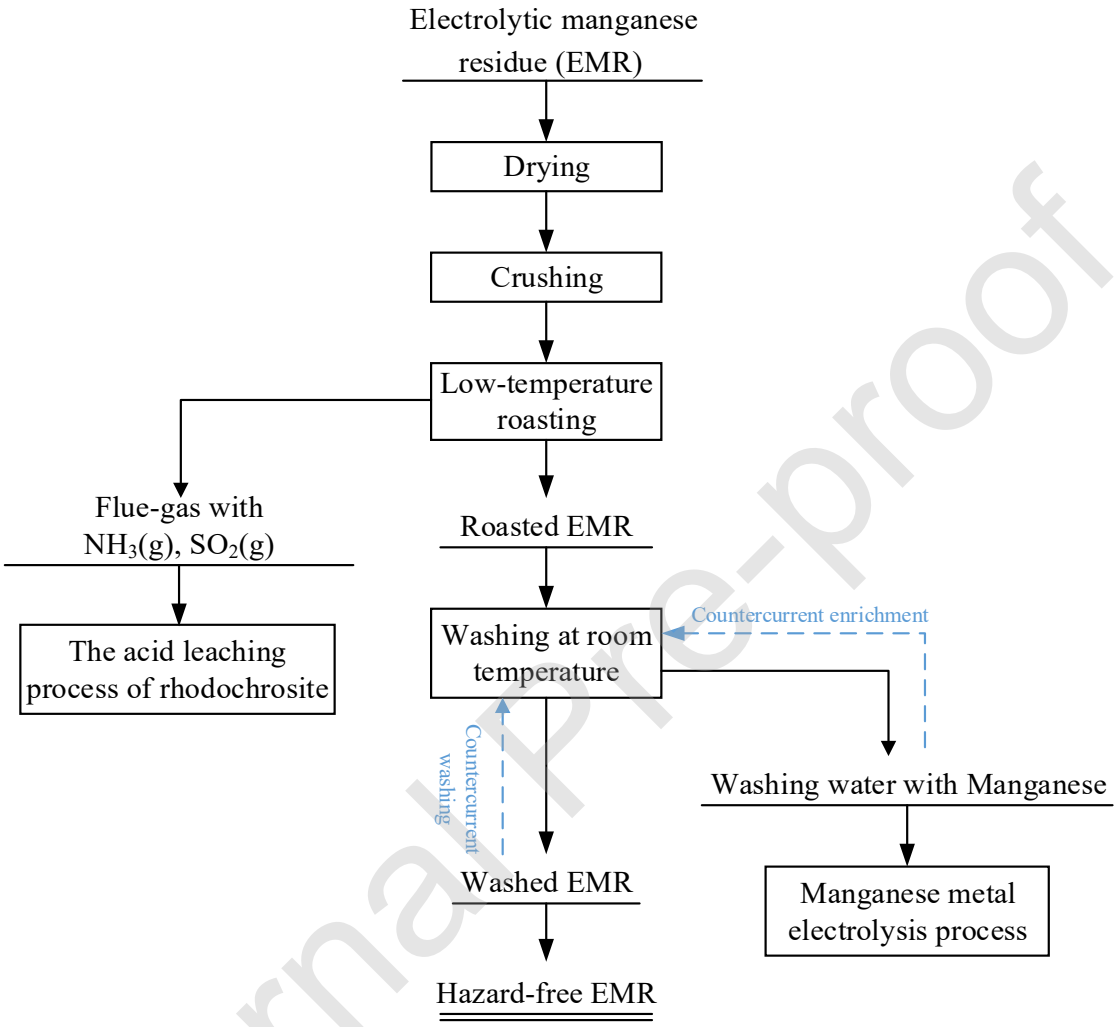

Fig. 10 Schematic flowsheet of the treatment of EMR by the low temperature roasting-water washing process

4. Conclusions

(1) The complete decomposition and transformation of the ammonium sulfate and pyrite phases in the EMR can be achieved by roasting at the following treatment

time/temperature conditions: 120 min / 550 °C, 60 min / 600 °C, 30 min / 650 °C;

(2) $R_{60min/600°C}$ has the highest manganese recovery rate. The roasted EMR was washed six times, and the content of manganese in the 6th washing solution was lower than 0.005 g/L. After 3 times of enrichment with $R_{60min/600°C}$, the content of manganese in the washing solution reaches 40.12 g/L, which satisfies the production demand of electrolytic manganese metal;

(3) The results of toxic leaching of EMR after treatment by the low temperature roasting-water washing process meet the requirements of GB 8978-1996, which confirms the hazard-free treatment of EMR is possible.

Author Contributions

Shichao He: Conceptualization, Methodology, Software, Investigation, Data Curation, Writing - Original Draft.

Benjamin P. Wilson: Writing - Review & Editing.

Mari Lundström: Writing - Review & Editing.

Zhihong Liu: Resources, Writing - Review & Editing, Supervision, Data Curation.

Declaration of interests

☒ The authors declare that they have no known competing financial interests or personal relationships that could have appeared to influence the work reported in this paper.

References

Aleksandrov, P.V., Medvedev, A.S., Milovanov, M.F., Imideev, V.A., Kotova, S.A., Moskovskikh, D.O., 2017. Molybdenum recovery from molybdenite concentrates by low-temperature roasting with sodium chloride. Inter. J. Miner. Process 161, 13-20. http://dx.doi.org/10.1016/j.minpro.2017.02.007.

Aleksandrov, P.V., Medvedev, A.S., Imideev, V.A., Moskovskikh, D.O., 2019. Nickel sulphide concentrate processing via low-temperature calcination with sodium chloride. Part I - Identifcation of interaction products. Miner. Eng. 134, 37-53. https://doi.org/10.1016/j.mineng.2019.01.001.

Bemana, H., Nadimi, S.R., 2017. Effect of sulfur doping on photoelectrochemical performance of hematite. Electrochim. Acta 229, 396-403. http://dx.doi.org/10.1016/j.electacta.2017.01.150.

Brantley, F., Rampacek, C., 1968. Manganese and iron recovery from leach solutions. US Patent, No. 3397130.

Cai, C., Luan, Y., Shi, X., Zhang, Y., 2017. $(NH_4)_2SO_4$ heterogeneous nucleation and glycerol evaporation of $(NH_4)_2SO_4$-glycerol system in its dynamic efflorescence process. Chem. Phys. 483-484, 140-148. http://dx.doi.org/10.1016/j.chemphys.2016.12.003.

Chen, J., Li, L., Chen, G., Peng, J., Srinivasakannan, C., 2017. Rapid thermal decomposition of manganese ore using microwave heating. J. Alloy. Comp. 699, 430-435. http://dx.doi.org/10.1016/j.jallcom.2016.12.379.

Cui, F., Mu, W., Wang, S., Xin, H., Shen, H., Xu, Q., Zhai, Y., Luo, S., 2018. Synchronous extractions of nickel, copper, and cobalt by selective chlorinating roasting and water leaching to low-grade nickel-copper matte. Sep. Purif. Technol. 195, 149-162. https://doi.org/10.1016/j.seppur.2017.11.071.

Dolezělová, M., Scheinherrová, L., Krejsová, J., Vimmrová, A., 2018. Effect of high temperatures on gypsum-based composites. Constr. Build. Mater. 168, 82-90. https://doi.org/10.1016/j.conbuildmat.2018.02.101.

Du, B., Zhou, C., Dan, Z., Luan, Z., Duan, N., 2014. Preparation and characteristics of steam-autoclaved bricks produced from electrolytic manganese solid waste. Constr. Build. Mater. 50, 291-299. http://dx.doi.org/10.1016/j.conbuildmat.2013.09.055.

Duan, N., Wang, F., Zhou, C., Zhu, C., Yu, H., 2010. Analysis of pollution materials generated from

electrolytic manganese industries in China. Resour. Conserv. Recy. 54, 506-511. http://dx.doi.org/10.1016/j.resconrec.2009.10.007.

Duan, N., Dan, Z., Wang, F., Pan, C., Zhou, C., Jiang, L., 2011. Electrolytic manganese metal industry experience based China's new model for cleaner production promotion. J. Clean. Prod. 19, 2082-2087.

http://dx.doi.org/10.1016/j.jclepro.2011.06.024.

Engbrecht, D.C., Hirschfeld, D.A., 2016. Thermal analysis of calcium sulfate dihydrate sources used to manufacture gypsum wallboard. Thermochim. Acta 639, 173-185.

http://dx.doi.org/10.1016/j.tca.2016.07.021.

Hagelstein, K., 2009. Globally sustainable manganese metal production and use. J. Environ. Manage. 90, 3736-3740.

http://dx.doi.org/10.1016/j.jenvman.2008.05.025.

Haynes, W.M., Lide, D.R., Bruno, T.J., 2015. CRC Handbook of Chemistry and Physics. 96th ed., CRC press, Boca Raton, pp 5-190.

Hou, P., Qian, J., Wang, Z., Deng, C., 2012. Production of quasi-sulphoaluminate cementitious materials with electrolytic manganese residue. Cem. Concr. Compos. 34, 248-254.

http://dx.doi.org/10.1016/j.cemconcomp.2011.10.003.

HSC Chemistry, 2019. HSC Chemistry 9.0: Reaction equations module. Outotec's chemical reaction and equilibrium software HSC Chemistry, Outotec company, Finland.

https://www.hsc-chemistry.com.

Huang, P., Deng, S., Zhang, Z., Wang, X., Chen, X., Yang, X., Yang, L., 2015. A sustainable process to utilize ferrous sulfate waste from titanium oxide industry by reductive decomposition reaction with pyrite. Thermochim. Acta 620, 18-27.

http://dx.doi.org/10.1016/j.tca. 2015.10.004.

Iucolano, F., Liguori, B., Aprea, P., Caputo, D., 2018. Thermo-mechanical behaviour of hemp fibers-reinforced gypsum plasters. Constr. Build. Mater. 185, 256-263.

https://doi.org/10.1016/j.conbuildmat.2018.07.036.

Jassim, E., Benson, S.A., Bowman, F.M., Seames, W.S., 2011. The influence of fragmentation on the behavior of pyrite particles during pulverized coal combustion. Fuel Process. Technol. 92, 970-976.

http://dx.doi.org/10.1016/j.fuproc.2010.12.018.

Jing, Z., Wu, S., 2004. Synthesis and characterization of monodisperse hematite nanoparticles modified by surfactants via hydrothermal approach. Mater. Lett. 58, 3637-3640. http://dx.doi.org/10.1016/j.matlet.2004.07.010.

Khanlariana, M., Rashchia, F., Saba, M., 2019. A modified sulfation-roasting-leaching process for recovering Se, Cu, and Ag from copper anode slimes at a lower temperature. J. Environ. Manage. 235, 303-309. https://doi.org/10.1016/j.jenvman.2019.01.079.

Li, R., Yin, J., Wang, W., Li, Y., Zhang, Z., 2014. Transformation of phosphorus during drying and roasting of sewage sludge, Waste Manage. 34, 1211-1216. http://dx.doi.org/10.1016/j.wasman.2014.03.022.

Li, C., Zhong, H., Wang, S., Xue, J., Zhang, Z., 2015. Removal of basic dye (methylene blue) from aqueous solution using zeolite synthesized from electrolytic manganese residue. J. Ind. Eng. Chem. 23, 344-352. http://dx.doi.org/10.1016/j.jiec.2014.08.038.

Li, Q., Liu, Q., Peng, B., Chai, L., Liu, H., 2016. Self-cleaning performance of TiO_2-coating cement materials prepared based on solidification/stabilization of electrolytic manganese residue. Cons. Build. Mater. 106, 236-242. http://dx.doi.org/10.1016/j.conbuildmat.2015.12.088

Li, J., Chen, Z., Shen, B., Xu, Z., Zhang, Y., 2017. The extraction of valuable metals and phase transformation and formation mechanism in roasting-water leaching process of laterite with ammonium sulfate. J. Clean. Prod. 140, 1148-1155. http://dx.doi.org/10.1016/j.jclepro.2016.10.050.

Li, J., Du, D., Peng, Q., Wu, C., Lv, K., Ye, H., Chen, S., Zhan, W., 2018. Activation of silicon in the electrolytic manganese residue by mechanical grinding-roasting. J. Clean. Prod. 192, 347-353. https://doi.org/10.1016/j.jclepro.2018.04.184.

Liu, X., Zhang, Q., Jiang, T., Yang, Y., Xu, B., He, Y., 2019. Improving gold recovery from a refractory ore via Na_2SO_4 assisted roasting and alkaline Na_2S leaching. Hydrometallurgy.185, 133-141. https://doi.org/10.1016/j.hydromet.2019.02.008.

Lu, J., Dreisinger, D., Glück, T., 2014. Manganese electrodeposition - A literature review. Hydrometallurgy 141, 105-116.

http://dx.doi.org/10.1016/j.hydromet.2013.11.002.

Luo, A., Fang, H., Xia, J., Lin, B., Jiang, Y., 2017. Mapping potentials of low-grade industrial waste heat in Northern China. Resour. Conserv. Recyc. 125, 335-348.

http://dx.doi.org/10.1016/j.resconrec.2017.06.018.

Mao, L., T-Raissi, A., Huang, C., Muradov, N., 2011. Thermal decomposition of $(NH_4)_2SO_4$ in presence of Mn_3O_4, Int. J. Hydrogen Energy 36, 5822-5827.

http://dx.doi.org/10.1016/j.ijh ydene.201 0.11.011.

Mei, G., Zhang, W., Zeng, B., Zeng, X., Li, G., Shi, J., Li, F., Jiang, Q., 2011. Technology of China manganese industry. Press of Central South University, Changsha. [in Chinese]

Middya, S., Layek, A., Dey, A., Ray P.P., 2014. Synthesis of nanocrystalline FeS_2 with increased band gap for solar energy harvesting. J. Mater. Sci. Technol. 30, 770-775.

http://dx.doi.org/10.1016/j.jmst.2014.01.005.

Mohamed, S., van der Merwe, E.M., Altermann, W., Doucet, F.J., 2016. Process development for elemental recovery from PGM tailings by thermochemical treatment: Preliminary major element extraction studies using ammonium sulphate as extracting agent. Waste Manage. 50, 334-345.

http://dx.doi.org/10.1016/j.wasman.2016.02.021.

Mu, W., Cui, F., Huang, Z., Zhai, Y., Xu, Q., S. Luo, 2018. Synchronous extraction of nickel and copper from a mixed oxide sulfide nickel ore in a low-temperature roasting system. J. Clean. Prod. 177, 371-377.

https://doi.org/10.1016/j.jclepro.2017.12.260.

Philias, J.M., Marsan, B., 1999. FTIR spectroscopic study and thermal and electrical properties of polymer electrolytes containing a cesium thiolate/disulfide redox couple. Electrochim. Acta 44, 2351-2363.

http://dx.doi.org/10.1016/S0013-4686(98)00357-0.

Sadik, C., Moudden, O., Bouari, A.E., Amrani, I. E., 2016. Review on the elaboration and characterization of ceramics refractories based on magnesite and dolomite. J. Asian Ceram. Soc. 4, 219-233.

http://dx.doi.org/10.1016/j.jascer.2016.06.006

Shen, P., Lu, L., He, Y., Wang, F., Hu, S., 2017. Hydration of quaternary phase-gypsum system, Constr. Build. Mater. 152, 145-153.
http://dx.doi.org/10.1016/j.conbuildmat.2017.06.179.

Shu, J., Liu, R., Liu, Z., Chen, H., Du, J., Tao, C., 2016a. Solidification/stabilization of electrolytic manganese residue using phosphate resource and low-grade MgO/CaO. J. Hazard. Mater. 317, 267-274.
http://dx.doi.org/10.1016/j.jhazmat.2016.05.076.

Shu, J., Liu, R., Liu, Z., Chen, H., Tao, C., 2016b. Simultaneous removal of ammonia and manganese from electrolytic metal manganese residue leachate using phosphate salt. J. Clean. Prod. 135, 468-475.
http://dx.doi.org/10.1016/j.jclepro.2016.06.141.

Shu J., Liu, R., Liu, Z., Chen, H., Tao, C., 2016c. Enhanced extraction of manganese from electrolytic manganese residue by electrochemical. J. Electroanal. Chem. 780, 32-37.
http://dx.doi.org/10.1016/j.jelechem.2016.08.033.

Shu, J., Wu, H., Liu, R., Liu, Z., Li, B., Chen, M., Tao, C., 2018a. Simultaneous stabilization/solidification of Mn^{2+} and NH_4^+-N from electrolytic manganese residue using MgO and different phosphate resource. Ecotoxicol. Environ. Safe. 148, 220-227.
http://dx.doi.org/10.1016/j.ecoenv.2017.10.027.

Shu, J., Liu, R., Wu, H., Liu, Z., Sun, X., Tao, C., 2018b. Adsorption of methylene blue on modified electrolytic manganese residue: Kinetics, isotherm, thermodynamics and mechanism analysis. J. Taiwan Ins. Chem. Eng. 82, 351-359.
https://doi.org/10.1016/j.jtice.2017.11.020.

Shu, J., Sun, X., Liu, R., Liu, Z., Wu, H., Chen, M., Li, B., 2019a. Enhanced electrokinetic remediation of manganese and ammonia nitrogen from electrolytic manganese residue using pulsed electric field in different enhancement agents. Ecotoxicol. Environ. Saf. 171, 523-529.
https://doi.org/10.1016/j.ecoenv.2019.01.025.

Shu, J., Wu, H., Chen, M., Wei, L., Wang, B., Li, B., Liu, R., Liu, Z., 2019b. Simultaneous optimizing removal of manganese and ammonia nitrogen from electrolytic metal manganese residue leachate using chemical equilibrium model. Ecotoxicol. Environ. Saf. 172, 273-280.
https://doi.org/10.1016/j.ecoenv.2019.01.071.

Standards, 1995. The State General Administration of the People's Republic of China for Quality Supervision and Inspection and Quarantine. Ammonium sulphate. The State Standard of the People's Republic of China, GB 535-1995, Standards Press of China, Beijing. [in Chinese]

Standards, 1996. The State Bureau of Environmental Protection and The State Bureau of Technical Supervision. Integrated wastewater discharge standard. The State Standard of the People's Republic of China, GB 8978-1996, Standards Press of China, Beijing. [in Chinese]

Standards, 2000. The State General Administration of the People's Republic of China for Quality Supervision and Inspection and Quarantine. Methods for chemical analysis of aluminate cement. The State Standard of the People's Republic of China, GB/T 205-2000, Standards Press of China, Beijing. [in Chinese]

Standards, 2007. The State Environmental Protection Administration. Solid waste-Extraction procedure for leaching toxicity-Acetic acid buffer solution method. The People's Republic of China Environmental Protection Industry Standards, HJ/T 300-2007, China Environmental Science Press, Beijing. [in Chinese]

Standards, 2009a. The Ministry of Environmental Protection. Water quality-Determination of cyanide-Volumetric and spectrophotometry method. The People's Republic of China Environmental Protection Industry Standards, HJ 484-2009, China Environmental Science Press, Beijing. [in Chinese]

Standards, 2009b. The Ministry of Environmental Protection. Water quality-Determination of ammonium nitrogen-Nessler's reagent spectrophotometry. The People's Republic of China Environmental Protection Industry Standards, HJ 535-2009, China Environmental Science Press, Beijing. [in Chinese]

Standards, 2017. The Ministry of Environmental Protection. Water quality-Determination of chromium (VI) - Flow injection analysis (FIA) and diphenylcarbazide spectrometric method. The People's Republic of China Environmental Protection Industry Standards, HJ 908-2017, China Environmental Science Press, Beijing. [in Chinese]

Tan, Z., Mei, G., Li, W., Zeng, K., Liang, R., Zeng, X., 2005. Metallurgy of manganese, Press of Central South University, Changsha. [in Chinese]

Wang, J., Peng, B., Chai, L., Zhang, Q., Liu, Q., 2013. Preparation of electrolytic manganese residue-ground granulated blast furnace slag cement. Powder Tech. 241, 12-18.

http://dx.doi.org/10.1016/j.powtec.2013.03.003.

Wu, F., Li, X., Zhong, H., Wang, S., 2016. Utilization of Electrolytic Manganese Residues in Production of Porous Ceramics. Int. J. Appl. Ceram. Technol. 13[3], 511-521. http://dx.doi.org/10.1111/ijac.12502.

Xin, B., Chen, B., Duan, N., Zhou, C., 2011. Extraction of manganese from electrolytic manganese residue by bioleaching. Bioresour. Technol. 102, 1683-1687. http://dx.doi.org/10.1016/j.biortech.2010.09.107.

Xu, F., Jiang, L., Dan, Z., Gao, X., Duan, N., Han, G., 2014. Water balance analysis and wastewater recycling investigation in electrolytic manganese industry of China - A case study. Hydrometallurgy 149, 12-22. http://dx.doi.org/10.1016/j.hydromet.2014.05.002.

Yan, H., Zhang, B., 2011. In vitro cytotoxicity of monodispersed hematite nanoparticles on Hek 293 cells. Mater. Lett. 65, 815-817. http://dx.doi.org/10.1016/j.matlet.2010.12.004.

Yang, C., Chen, Y., Peng, P., Li, C., Chang, X., Wu, Y., 2009. Trace element transformations and partitioning during the roasting of pyrite ores in the sulfuric acid industry. J. Hazard. Mater. 167, 835-845. http://dx.doi.org/10.1016/j.jhazmat.2009.01.067.

Yang, C., Lv, X., Tian, X., Wang, Y., Komarneni, S., 2014. An investigation on the use of electrolytic manganese residue as filler in sulfur concrete. Constr. Build. Mater. 73, 305-310. http://dx.doi.org/10.1016/j.conbuildmat.2014.09.046.

Yang, L., Dai, L., Li, H., Hu, H., Zhuang, Y., Liu, K., Pu, C., Hong, M., 2018. Pressure-induced structural phase transition and dehydration for gypsum investigated by Raman spectroscopy and electrical conductivity. Chem. Phys. Lett. 706, 151-157. https://doi.org/10.1016/j.cplett.2018.06.007.

Zhang, W., Cheng, C., 2007. Manganese metallurgy review. Part I: Leaching of ores/secondary materials and recovery of electrolytic/chemical manganese dioxide. Hydrometallurgy, 89, 137-159. http://dx.doi.org/10.1016/j.hydromet.2007.08.010.

Zhou, C., Du, B., Wang, N., Chen, Z., 2014. Preparation and strength property of autoclaved bricks from electrolytic manganese residue. J. Clean. Prod. 84, 707-714.

http://dx.doi.org/1 0.1016/j.jclepro.2014.01.052.